Registry No. BeH_2, 7787-52-2; BH_3, 13283-31-3; CH_4, 74-82-8; NH_3, 7664-41-7; H_2O, 7732-18-5; SiH_4, 7803-62-5; PH_3, 7803-51-2; PH_5, 13769-19-2; SH_2, 7783-06-4; SH_4, 51621-86-4; SH_6, 51715-67-4; ClH_3, 66653-01-8; ClH_5, 66653-00-7; ArH_6, 66674-95-1.

References and Notes

(1) M. B. Hall, *J. Am. Chem. Soc.*, to be submitted for publication.
(2) R. J. Gillespie and R. S. Nyholm, *Q. Rev., Chem. Soc.*, **11**, 339 (1957); R. J. Gillespie, *Angew. Chem., Int. Ed. Engl.*, **6**, 819 (1967).
(3) M. Wolfsberg and L. Helmholz, *J. Chem. Phys.*, **20**, 837 (1952); R. Hoffmann and W. N. Lipscomb, *ibid*, **36**, 2179, 3489 (1962); **37**, 2873 (1962).
(4) L. C. Allen and J. D. Russell, *J. Chem. Phys.*, **46**, 1029 (1967); L. C. Allen, *Theor. Chim. Acta*, **24**, 177 (1972).
(5) B. M. Gimarc, *J. Am. Chem. Soc.*, **92**, 266 (1970); **93**, 593, 815 (1971).
(6) L. S. Bartell, *Inorg. Chem.*, **5**, 1635 (1966); *J. Chem. Educ.*, **45**, 754 (1968); L. S. Bartell and V. Plato, *J. Am. Chem. Soc.*, **95**, 3097 (1973).
(7) A. D. Walsh, *J. Chem. Soc.*, 2260, 2266, 2288, 2296, 2301, 2306 (1953).
(8) K. Ruedenberg, *Rev. Mod. Phys.*, **34**, 326 (1962).
(9) C. J. Ballhausen and H. B. Gray, *Inorg. Chem.*, **1**, 111 (1962); L. C. Cusachs, *J. Chem. Phys.*, **43**, S157 (1965).
(10) W. J. Hehre, R. Ditchfield, R. F. Stewart, and J. A. Pople, *J. Chem. Phys.*, **52**, 2769 (1970).
(11) R. S. Mulliken, *J. Chem. Phys.*, **23**, 1833, 1841, 2338, 2343 (1955).
(12) J. P. Lowe, *J. Am. Chem. Soc.*, **96**, 3759 (1974).
(13) A. R. Gregory and M. N. Paddon-Row, *J. Am. Chem. Soc.*, **98**, 7521 (1976); P. Caramella, K. N. Houk, and L. N. Domelsmith, *ibid.*, **99**, 4511 (1977).
(14) C. C. Levin, *J. Am. Chem. Soc.*, **97**, 5649 (1975); W. Cherry and N. Epiotis, *J. Am. Chem. Soc.*, **98**, 1135 (1975).
(15) M. F. Guest, M. B. Hall, and I. H. Hillier, *J. Chem. Soc., Faraday Trans. 2*, 1829 (1973); L. Radom and H. F. Schaefer III, *Aust. J. Chem.*, **28**, 2069 (1975); R. Gleiter and A. Veillard, *Chem. Phys. Lett.*, **37**, 33 (1976); S. R. Ungemach and H. F. Schaefer III, *ibid.*, **38**, 407 (1976).
(16) M. M. L. Chen and R. Hoffmann, *J. Am. Chem. Soc.*, **98**, 1647 (1976).
(17) R. Hoffmann, J. M. Howell, and E. L. Muetterties, *J. Am. Chem. Soc.*, **94**, 3047 (1972); A. Strich and A. Veillard, *ibid.*, **95**, 5574 (1973); A. Rauk, L. C. Allen, and K. Mislow, *ibid.*, **94**, 3035 (1972).
(18) L. S. Bartell and R. M. Gavin, Jr., *J. Chem. Phys.*, **48**, 2466 (1968).
(19) L. Pauling, "The Nature of the Chemical Bond", 3rd ed, Cornell University Press, Ithaca, N.Y., 1960, p 120; C. A. Coulson, "Valence", 2nd ed, Oxford University Press, Oxford, 1961, pp 163, 179, 221.

Contribution from the Department of Chemistry, Texas A&M University, College Station, Texas 77843

Photoelectron Spectra of Substituted Chromium, Molybdenum, and Tungsten Pentacarbonyls. Relative π-Acceptor and σ-Donor Properties of Various Phosphorus Ligands

LINTON W. YARBROUGH, II,[1] and MICHAEL B. HALL*

Received December 29, 1977

The UV photoelectron spectra (PES) of the transition-metal complexes $LM(CO)_5$, where M = Cr, Mo, or W and L = PEt_3, PMe_3, $P(NMe_2)_3$, $P(OEt)_3$, $P(OMe)_3$, or PF_3, are reported and compared with the PES of the uncoordinated ligands. Particular emphasis is placed on the assignment of the metal d orbital band components, the M–P bond, and the P nonbonding pair in the free ligand. The ability of the ligands to split the t_{2g} orbitals of the parent hexacarbonyl into the e and b_2 components falls in the order $PEt_3 \sim PMe_3 > P(NMe_2)_3 > P(OEt)_3 \sim P(OMe)_3 > PF_3$ and follows the inverted order of π-acceptor ability of these ligands. The σ-donor ability is reflected in the ionization potential (IP) of the M–P bond and falls in the order $PEt_3 \sim PMe_3 > P(OEt)_3 \sim P(OMe)_3 > P(NMe_2)_3 > PF_3$. Comparisons of the free and complexed ligands allow us to make definitive assignments of the PES bands of the free ligands, assignments about which there has recently been considerable controversy. The spin–orbit coupling (SOC) parameters of the W complexes remain unexpectedly constant through this series of ligands rather than decreasing as their π-acceptor ability increases. We attribute this constancy to the ability of CO to release electron density to the metal, thus, compensating for loss of density as the π-acceptor ability of L increases. Therefore, the total delocalization of the metal remains constant. The σ/π parameters derived from the PES are also compared with those from CO force constants. Fenske–Hall molecular orbital (MO) calculations were done on the Cr complexes of PMe_3, $P(NMe_2)_3$, $P(OMe)_3$, and PF_3 and the results of these calculations support our assignments.

Introduction

Photoelectron spectroscopy (PES) has proven to be a valuable tool in the elucidation of the electronic structure of molecules.[2] Previous work by M.B.H. has shown the value of comparing the PES of first- and third-row transition-metal complexes.[3] The effect of spin–orbit coupling on the spectra in the case of $XRe(CO)_5$ species provided a definitive assignment and a measure of the total delocalization of the metal d electrons.

In this work we have undertaken a study of the PES of $LM(CO)_5$ systems where M is a group 6B metal (Cr, Mo, or W) and L is a phosphorus ligand (PEt_3, PMe_3, $P(NMe_2)_3$, $P(OEt)_3$, $P(OMe)_3$, or PF_3). Although there have been a number of recent papers dealing with the relative π acceptor and σ donor properties of the phosphine and phosphite ligands in these pentacarbonyls, most of the conclusions about these electronic properties have been based on the measurements of CO stretching frequencies[4] or ^{183}W–^{31}P coupling constants.[4g,5] There have been only a few studies on the electronic structure via more direct measurements such as PES.[6] These PES studies have also been under lower resolution than the results to be reported here.

The relative π-acceptor properties of these ligands should be reflected in the degree to which the t_{2g} of the parent hexacarbonyl is split into an e and b_2. In the case of tungsten the e is further split by the spin–orbit coupling into an e′ and e″ of the double group C_{4v}*.[3] Since the b_2 is also of e″ symmetry under the spin–orbit Hamiltonian, there is some interaction between it and the other e″ component. As we have shown previously,[3] a study of this effect can increase our confidence in a particular assignment and provide us with a measure of the total delocalization of the metal d electrons.

The relative σ-donor strength of ligands should be reflected to a large degree by the ionization potential (IP) of the M–P bonding molecular orbital (MO). The comparison between the free and coordinated ligand spectra also provides a definitive assignment for the P lone pair (donor orbital), since it will be perturbed more severely than the other ligand orbitals on coordination. There has been considerable controversy recently concerning the assignment of several of these ligands,[7] which is resolved by this work.

Experimental and Theoretical Section

Preparation. All solvents were dried over molecular sieves and purged with N_2. Where possible, all materials were handled in an

0020-1669/78/1317-2269$01.00/0

Table I. Ligand Geometry Data

ligand	bond lengths, Å		bond angles, deg		dihedral angles, deg	
$P(CH_3)_3$	P-1	1.846	M-P-1	118.9	M-P-1-2	0
	1-2	1.096	P-1-2	109.6	M-P-1-3	120
			1-P-1′	98.6	M-P-1-4	240
$P[N(CH_3)_2]_3$	P-1	1.648	M-P-1	112.7	M-P-1-2	60
	1-2	1.448	P-1-2	118.3	M-P-1-3	240
	2-5	1.096	2-1-3	111.8	P-1-2-5	180
			1-2-5	109.6	P-1-2-6	60
			1-P-1′	106.1	P-1-2-7	300
$P(OCH_3)_3$	P-1	1.574	M-P-1	116.3	M-P-1-2	0
	1-2	1.410	P-1-2	129.1	P-1-2-5	180
	2-5	1.096	1-2-5	109.6	P-1-21-6	60
			1-P-1′	101.8	P-1-2-7	300
PF_3	P-1	1.570	M-P-1	119.5		
			1-P-1′	97.8		

inert atmosphere. Published procedures[8] were followed for the preparation of all compounds except the PF_3 derivatives. All complexes were purified by sublimation or recrystallization and were verified by melting/boiling point or ^1H NMR or IR spectroscopy.

The $PF_3M(CO)_5$ compounds were prepared by the slow, simultaneous addition of fairly dilute CH_2Cl_2 solutions of $(Et_3O)(BF_4)$[9] in twofold excess and $[NH_4][ClM(CO)_5]$[10] to a PF_3-saturated CH_2Cl_2 solution cooled to 0 °C. The additions were done under an N_2 blanket while concurrently bubbling PF_3 through the cooled CH_2Cl_2. After the additions were complete, the volatiles were removed under high vacuum, while maintaining the reaction mixture at −10 °C. The flask was then allowed to slowly warm to room temperature, while the remaining volatile components were trapped at −25 °C. Overnight pumping of the trap, held at −15 °C, removed all contaminants and the remaining material proved to be the desired product. Although the yield is low, this procedure avoids the formation of any di- or trisubstituted complexes.

Spectroscopy. The PE spectra were taken on a Perkin-Elmer Model PS-18 photoelectron spectrometer, modified by the addition of a Tracor Northern Model TN-1706 multichannel analyzer. By making multiple passes through the region of interest, we were able to significantly improve the signal/noise. The data from the channels, which are spaced at 0.02-eV intervals, were used to deconvolute the d envelope into its components. The full spectra were recorded as a single slow sweep using the standard PS-18 recorder system. The argon line was used as the single internal standard, but the instrument was calibrated periodically using both MeI and Ar. The resolution was always better than 30 meV for the Ar $^2P_{3/2}$ line.

Deconvolution. The splitting of the d bands was resolved by fitting the data from the multichannel analyzer to asymmetric Gaussian peaks. The ratios of the left to right half-widths were fixed at the value obtained by fitting a single asymmetric Gaussian to the d band of $Cr(CO)_6$ (ratio = 0.467). It was further assumed that, when the t_{2g} band was split into an e and b_2, the intensity ratio would be 2 to 1. These assumptions can be justified from our work on Mn and Re complexes,[3] where the larger e–b_2 splitting and spin–orbit coupling made these assumptions unnecessary. Thus, for the Cr and Mo complexes, a single amplitude factor, a single half-width, a single overall band position, and the e–b_2 splitting were varied to fit the data (75 to 100 points). For the W complexes a fifth parameter, the value of the spin–orbit coupling, was introduced. The equations relating the final IP's to the value of the e–b_2 splitting and the spin–orbit coupling have been presented previously.[3]

Theoretical. The MO calculations on the Cr complexes of PMe_3, $P(NMe_2)_3$, $P(OMe)_3$, and PF_3 were performed by the approximate nonempirical method of Fenske and Hall.[11] The Cr(0) functions were those of Richardson[12] except for the 4s and 4p for which we used exponents of 2.0, a value which maximized the σ overlap with the ligands.[13] The C, N, O, and P functions were taken from the double ζ functions of Clementi[14] and reduced to a single ζ[13] except for the valence p, for which we retained the double ζ function. The exponent of H was taken as 1.2. The functions on each atom were made orthogonal by the Schmidt procedure. The geometries for the ligands were idealized to C_{3v} symmetry from published structural studies.[15] The bond length and angles for the CH_3 groups were those reported for MeOH.[16] The geometries are presented in Table I, wherein the numbering system refers to Figure 1, and the A–B–C–D dihedral angle refers to the clockwise rotational difference between AB and CD when looking down the BC axis. The Cr–P, Cr–C, and carbonyl C–O bond lengths were also literature values[17] and were kept constant in each complex so that the calculated differences could be limited to energetic effects and would not include an inherent geometric bias. A Mulliken population analysis was used to determine the gross charges on the atoms and populations of individual atomic orbitals.

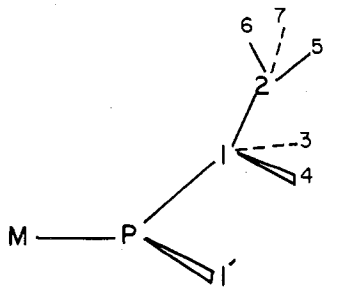

Figure 1. Ligand numbering system. (Note: only one of the three C_{3v} symmetry related phosphorus substituents is shown.)

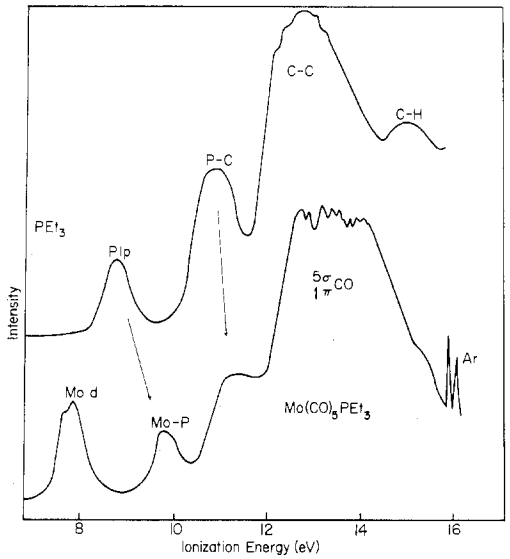

Figure 2. PES of $PEt_3/PEt_3Mo(CO)_5$.

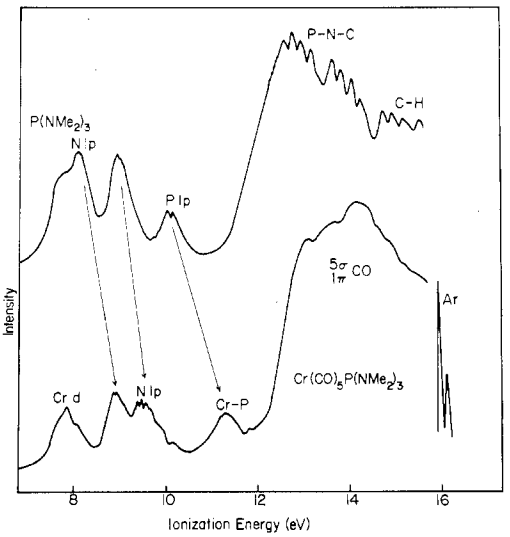

Figure 3. PES of $P(NMe_2)_3/P(NMe_2)_3Cr(CO)_5$.

Results and Discussion

Free vs. Coordinated Ligand. Several representative PES are shown in Figures 2–5, and each contains a spectrum of the free ligand and the complex. Since the exact conformational geometry is unknown for most of the ligands and

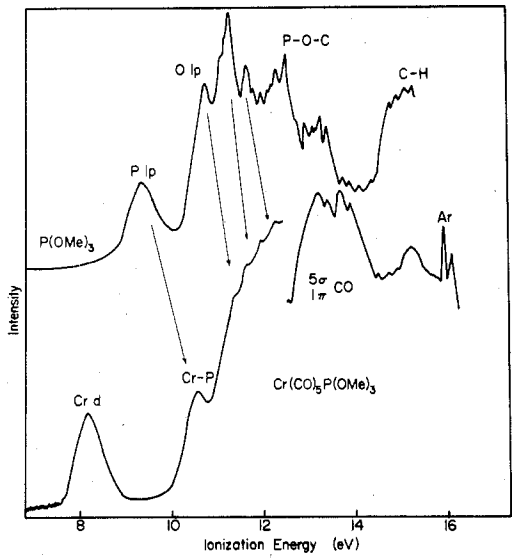

Figure 4. PES of $P(OMe)_3/P(OMe)_3Cr(CO)_5$.

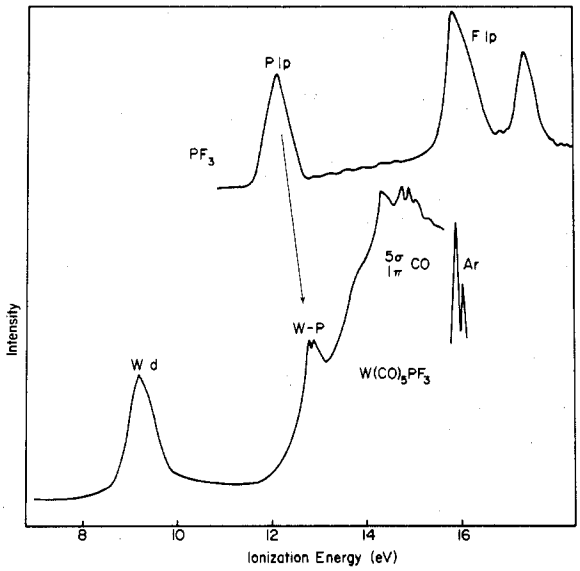

Figure 5. PES of $PF_3/PF_3W(CO)_5$.

complexes, we have made assignments of the bands according to their major atomic components. To assume a particular point group and make assignments using the symmetry designations would only be misleading. In Figure 2 the first band of the free PEt_3 corresponds to the P lone pair, the second corresponds to the symmetry-adapted P–C combinations, and the remaining broad overlapping bands correspond to the C–C and C–H interactions. In the complex the band around 8 eV is the Mo d envelope; the next is the Mo–P bond, followed by the P–C bonds and, finally, the CO region overlapping the C–C and C–H bands. All of the ligand bands increase in IP upon coordination, but the P lone pair increases the most because of the direct M–P interaction. The PES of free and coordinated tris(dimethylamino)phosphine is shown in Figure 3. The spectrum of the free ligand shows four bands below 11 eV; three are assigned to N lone pair orbitals and one to the P lone pair. Much of the recent controversy has concerned these band assignments. We feel justified in assigning the highest IP band as the P lone pair because upon coordination this band is stabilized more than the others. The larger stabilization for the P lone pair compared to the N lone pairs is also supported by the MO calculations. However, the approximate MO calculations indicate substantial mixing of the P and N lone pair orbitals, so this band probably contains

Table II. Free Ligand and Complex PES Data (eV)

compd		a_1 free ligand	a_1 complex	Δ coordination	metal d maxima
PEt_3	Cr	8.52	9.63	1.11	7.6
	Mo	8.52	9.63	1.11	7.7
	W	8.52	9.71	1.19	7.8
Av		8.52	9.66	1.14	
PMe_3	Cr	8.79	9.87	1.08	7.6
	Mo	8.79	9.84	1.05	7.7
	W	8.79	9.92	1.13	7.9
Av		8.79	9.88	1.09	
$P(NMe_2)_3$	Cr	10.01	11.07	1.06	7.6
	Mo	10.01	11.03	1.02	7.8
	W	10.01	11.14	1.13	7.9
Av		10.01	11.08	1.07	
$P(OEt)_3$	Cr	9.15	10.27	1.12	7.9
	Mo	9.15	10.30	1.15	8.0
	W	9.15	10.34	1.19	8.1
Av		9.15	10.30	1.15	
$P(OMe)_3$	Cr	9.21	10.33	1.12	8.0
	Mo	9.21	10.35	1.14	8.1
	W	9.21	10.36	1.15	8.2
Av		9.21	10.35	1.14	
PF_3	Cr	12.20	12.55	0.35	8.7
	Mo	12.20	12.52	0.37	8.8
	W	12.20	12.60	0.40	8.9
Av		12.20	12.57	0.37	

substantial N character, at least in the free ligand. The assignments of the remaining bands are indicated on Figure 3. A particularly important point is that the N lone pairs are lower in IP than the P lone pair. Our results support the assignments of Cowley et al.,[7a] but not those of Worley.[7b] Figure 4 shows the PES of $P(OMe)_3$ and its Cr complex. The assignments are indicated and, again, it should be noticed that the P lone pair is stabilized upon coordination to a greater extent than any other ligand orbital. However, unlike the previous N compound, the O lone pairs in the phosphite have an IP higher than that of the P lone pair. This conclusion differs from the previous interpretation of the free ligand spectrum.[7a] Figure 5 contains the PF_3 spectra and shows the P lone pair at higher IP than that of the other ligands and the F lone pair at a very high IP. On coordination the P lone pair moves up in IP, but not as much as in the other ligands.

The IP values for the P lone pair, the M–P bonds, and the approximate maxima of the multicomponent metal d envelopes are given in Table II. Our assignments of the P lone pair and M–P bond are supported by the rather constant change on coordination which is ~1.1 eV for each ligand except PF_3. These data allow us to establish an order of σ-donor ability as $PEt_3 \sim PMe_3 > P(OEt)_3 \sim P(OMe)_3 > P(NMe_2)_3 > PF_3$ based upon both the free and complexed ligand a_1 IP's. The PF_3 ligand stands out as a much weaker donor because of both its higher IP and its smaller change on coordination. From inductive arguments one might expect the σ-donor trend to parallel the electronegativity of the P substituents ($R < NR_2 < OR < F$).. However, the donor properties as reflected by the IP are reversed for NR_2 and OR. This reversal can be accounted for by considering direct interaction between the lone pair on P and the orbitals on its substituents, as shown in Figure 6. In PF_3 the highly electronegative F's place the P diagonal term rather low. The P is then destabilized somewhat by P–F interactions, but because the F orbitals are much lower in energy, they interact only very weakly with the P orbitals. Thus, the electronegativity effects of F dominate the energy of the P a_1 orbitals. In the phosphites the P lone pair diagonal energy rises compared to that in PF_3 due to the less electronegative oxygen. In addition, the close proximity of the oxygen (both lone pairs and P–O bonding) orbitals to the P destabilizes the P a_1 considerably. In the case of the

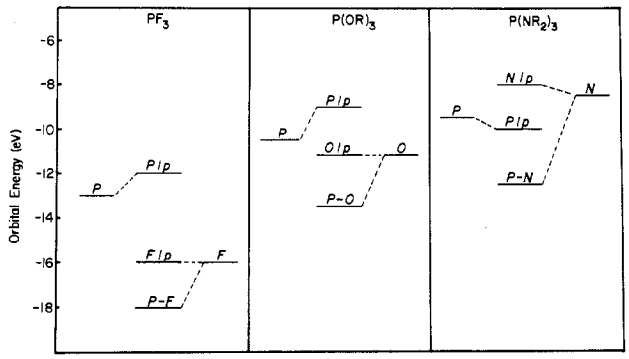

Figure 6. MO diagrams for PF_3, $P(OR)_3$, and $P(NR_2)_3$.

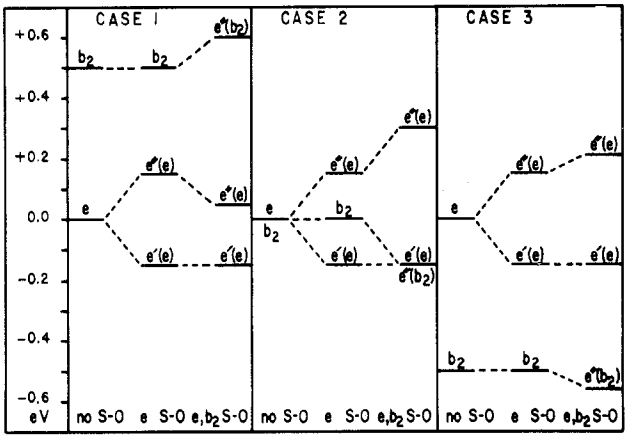

Figure 7. MO diagrams for three possible cases of spin–orbit coupling in $LM(CO)_5$ compounds.

(dialkylamino)phosphine, the P diagonal term again rises because of the decrease in the electronegativity, but now the N orbitals are above the P diagonal term so that their interaction stabilizes the P a_1 orbital. Thus, the direct interaction of the P lone pair with the heteroatom's orbitals accounts for the reversal in the σ-donor properties of $P(OR)_3$ and $P(NR_2)_3$ ligands. The MO diagram in Figure 6 was constructed by placing the MO energies at their experimental values. The MO calculations and the experimental assignments were then used to establish the qualitative trends in the diagonal terms.

Resolution of d Bands. We have also taken high-resolution spectra of the metal d bands with the multichannel analyzer described earlier. In a hexacarbonyl such as $Cr(CO)_6$, the electronic configuration is t_{2g},[6] and there is a single band observed at 8.5 eV corresponding to this orbital. When the symmetry is reduced by replacing one of the carbonyls with a different ligand, the t_{2g} band splits into e and b_2 components. Although the full symmetry of the molecules considered here is much lower than C_{4v}, our calculations on several $LCr(CO)_5$ compounds indicate that the splitting of the e bands due to symmetry components lower than C_{4v} is less than 0.001 eV. Thus, for the metal orbitals the symmetry is well approximated by C_{4v}. If the unique ligand is a better π acceptor than CO, one would expect the e IP to be greater than the b_2 IP, while if it is a poorer π acceptor, one would expect the reverse order. For W compounds there is an additional perturbation due to spin–orbit coupling (SOC), which splits the e into e′ and e″ (C_{4v} double group) and also perturbs the b_2 since it is now of e″ symmetry. The complete equations for this effect have been presented previously[3] and the results are summarized in Figure 7. Case 1 of Figure 7 shows the scheme for the b_2 level above the e level; in this case the splitting between the first and second IP must be greater than the splitting between second and third IP. As the b_2 level approaches the e level, the splitting between the second and third IP decreases until they are equal (case 2). As the b_2 level becomes more stable than the e (case 3, Figure 7), the splitting between the second and third IP increases while the splitting between the first and second decreases. Only in case 3 can the splitting between the first and second IP be equal to or less than the splitting between the second and third IP. In addition to providing an aid to the assignment on the basis of the splitting pattern, the value of the spin–orbit coupling parameter from the deconvolution of the W spectra provides us with a measure of the overall delocalization of the metal electrons. The smaller the SOC parameter, the more delocalized the metal d electrons are.

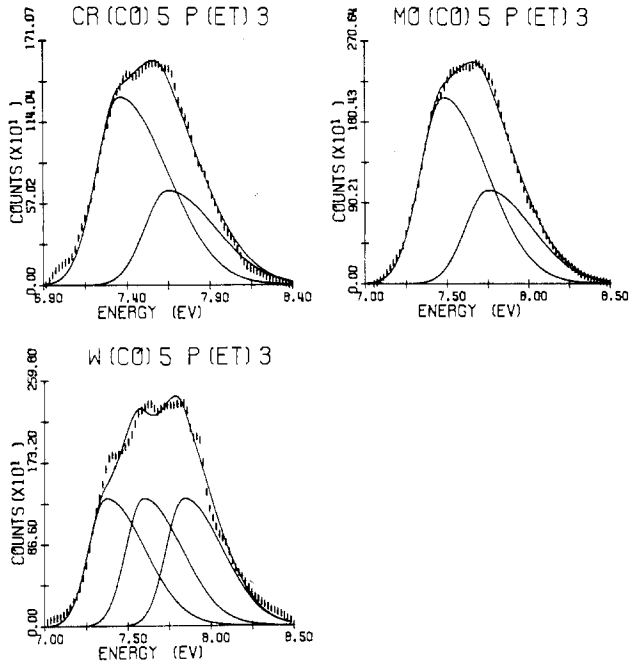

Figure 8. Deconvolution of the metal d band in $PEt_3M(CO)_5$.

The spectra and the computer curve fits for $PEt_3M(CO)_5$, M = Cr, Mo, and W, are shown in Figure 8. The vertical tick marks are the experimental data. The two (or three) components and their sum are shown by the solid lines. The observed bands clearly show a splitting of d orbitals, and, within the constraints described earlier, they can only be deconvoluted with precision by assuming $IP_e < IP_{b_2}$. This order and only this order can produce three approximately equally spaced peaks as is seen in the W spectrum. Although these deconvolutions could have been done without the applied constraints, which would have improved the curve fit, the constraints were necessary for some of the other spectra. Therefore, the constraints were applied to all deconvolutions so that valid comparisons could be made.

The metal d band spectra and deconvolutions of $W(CO)_6$ and the remaining $LW(CO)_5$ complexes are shown in Figure 9. In the phosphorus compounds the left and center bands are the spin–orbit split e orbitals while the right band is the b_2. In $W(CO)_6$ the orbitals are split by SOC only. In these W compounds the overall fit between the experimental and calculated curves is less than perfect because of the constraints applied, but the individual peaks do fall under the band maxima. On going from PEt_3 to PMe_3 we see a similar but less well resolved band with a somewhat smaller e–b_2 splitting. The band width and splitting decrease further in the $P(NMe_2)_3$ compound, and both decrease further still in the $P(OEt)_3$ complex although a splitting at the top of the band and a shoulder on the low-IP side can still be discerned. Further narrowing and an absence of obvious splitting are seen in the $P(OMe)_3$ spectrum. Finally, the PF_3 compound exhibits the narrowest band and smallest splitting, which is consistent with its known π-acceptor ability.

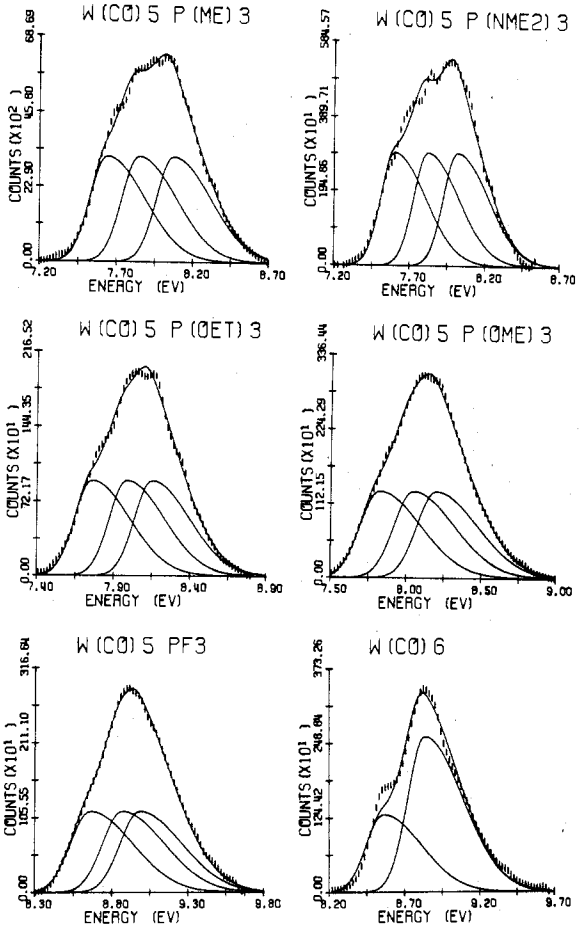

Figure 9. Deconvolution of the metal d band in $LW(CO)_5$ and $W(CO)_6$.

Table III. Orbital Splittings and W SOC Constants (eV)

	e–b_2				W
ligand	Cr	Mo	W	Av	SOC
PMe_3	−0.29	−0.29	−0.28	−0.29	0.17
PEt_3	−0.29	−0.27	−0.30	−0.29	0.18
$P(NMe_2)_3$	−0.24	−0.22	−0.24	−0.23	0.18
$P(OMe)_3$	−0.23	−0.20	−0.19	−0.21	0.18
$P(OEt)_3$	−0.20	−0.19	−0.21	−0.20	0.18
PF_3	−0.16	−0.20	−0.15	−0.17	0.16

The final values for e–b_2 splittings and W SOC parameters are shown in Table III. The standard error from the statistics of the deconvolution is less than 0.01 eV except for the PF_3. The uniformity of the splittings for each ligand with three different metals gives support to our values, especially, since each deconvolution was independently done without information from the others. The largest variation occurs in the PF_3 compounds which have the smallest e–b_2 splittings. The large Mo–PF_3 value may be due to the neglect of Mo spin–orbit coupling which becomes more important as the e–b_2 splitting decreases. A general overview of π-acceptor ability for each ligand type can be obtained from the average splittings: PR_3 (−0.29 ± 0.01) < $P(NR_2)_3$ (−0.23 ± 0.01) < $P(OR)_3$ (−0.20 ± 0.01) < PF_3 (−0.17 ± 0.03). This series parallels the relative electronegativity of the phosphorus substituent.

Also in Table III are listed the SOC constants obtained from the deconvolution of the W complexes. One might expect that the concomitant loss in metal electron density on increasing the π-acceptor ability of L would be reflected in decreasing SOC constants. However, this is not seen, as the complexes show a rather constant value in this parameter, and no apparent trend is evident. We believe this behavior is due to the very flexible M–CO π bond, which can release density into the metal as the acceptor ability of the phosphorus ligand increases. Thus, the CO's are acting as electron reservoirs and keep the overall metal d electron delocalization constant as shown by the SOC parameters.

Table IV. Deconvolution Results for $PF_3W(CO)_5$ (eV)

	e–b_2	SOC
case 3	−0.149 ± 0.005	0.161 ± 0.003
case 1	+0.198 ± 0.116	0.131 ± 0.078

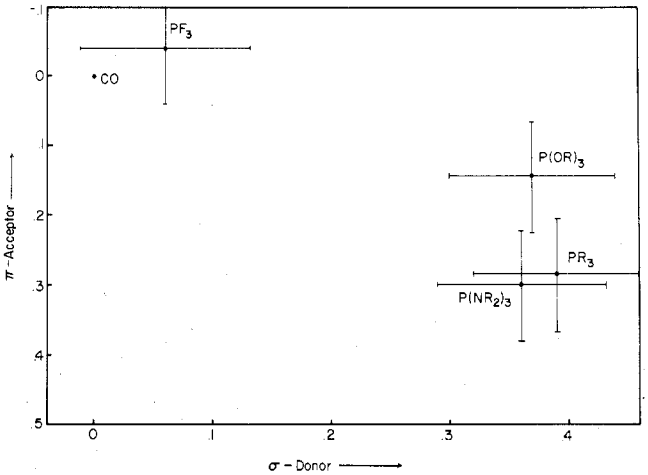

Figure 10. σ–π force constant analysis.

Our results for the PF_3 complexes deserve some additional comment, since they imply that PF_3 is a weaker π acceptor than CO. As shown in Table III, the e–b_2 splitting is rather small for the PF_3 ligand. From the conclusion of Figure 7, we recall that if the e level is below the b_2, one should observe a single band followed by two closely spaced ones. Thus, if the e–b_2 order were reversed in the PF_3 complexes, the spectra should resemble $W(CO)_6$ with a prominant shoulder at low IP. In fact the d band appears as a single envelope without any apparent structure. This shape is most readily explained by assuming the e level is above b_2 (case 3, Figure 7). Further quantitative evidence for this conclusion comes from our deconvolution program. The program can be forced to obtain the best possible fit of the spectra with a positive e–b_2 splitting (case 1, Figure 7). The best parameters for both cases and their standard error are shown in Table IV. The standard errors for both the e–b_2 splitting and the SOC parameter are statistically larger for case 1. In addition the SOC parameter itself is unacceptably small for a tungsten pentacarbonyl. We are forced to conclude that the e–b_2 splitting is negative and that PF_3 is a similar but weaker π acceptor than CO. In previous work on $M(PF_3)_6$ and $M(CO)_6$ complexes[18] Nixon observed the d band envelope at larger IP for PF_3 complexes and concluded that PF_3 has a slightly greater overall electron-withdrawing effect. We see a similar effect for the monosubstituted complex. However, our calculations suggest that this is due not to a greater electron-withdrawing effect for PF_3 but to the fact that this ligand, with the three very electronegative F's withdrawing charge from the P, presents a large electrostatic stabilization energy to the metal d electrons.

Probably the most widely used method for obtaining relative σ and π characteristics of ligands is based on a Graham analysis[19] of carbonyl force constants. Using literature values of IR frequencies,[4] we have obtained the Cotton–Kraihanzel force constants[20] and analyzed them according to the method of Graham. The results are shown in Figure 10. The error limits are those suggested by Graham and are probably

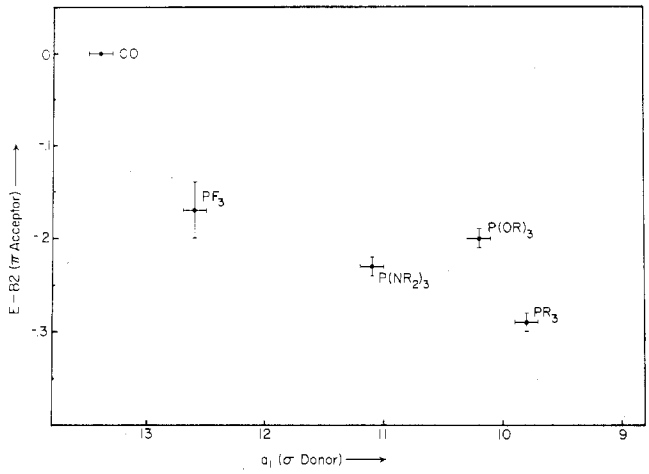

Figure 11. σ–π PES analysis.

conservative. Thus PF_3 and CO are of identical donor/acceptor characteristics within the error limits, and the clustering of the remaining ligands prevents any definitive ordering of their characteristics. However, the same type of plot can be constructed using e–b_2 splittings as a measure of π-acceptor ability and the M–P a_1 IP to define σ-donor ability.

This plot is shown in Figure 11 where the error bars (standard deviations) are considerably smaller than in Figure 10. The smaller error bars arise in large part from the fact that we are making direct experimental measurements of the π-acceptor/σ-donor properties, while a Graham-type analysis involves the reduction of the experimental frequency to approximate force constants and then the reduction of these to approximate π and σ parameters. Figure 11 shows that PF_3 is a better σ donor and poorer π acceptor than CO and establishes, without the overlap of the error limits, scales of relative acceptor and donor ability of the three classes of P ligands.

Our conclusion concerning the π-acceptor ability of PF_3 compared to CO is in agreement with the thermochemical bond energies.[21] These results show that the M–CO and M–PF_3 bonds are of nearly equal strength. Since PF_3 is a better σ donor than CO, a conclusion supported by this and most other work, it is reasonable that it should be a poorer π acceptor in order to have a overall bond strength equal to that of CO. If PF_3 were both a better σ donor and a better π acceptor than CO, one would expect a stronger overall M–PF_3 bond, a result in disagreement with the thermochemical studies.[21]

We also have done some approximate MO calculations on uncoordinated PMe_3, $P(NMe_2)_3$, $P(OMe)_3$, and PF_3 and the Cr complex of each. The calculations are in excellent qualitative agreement with our MO assignments made earlier and with the observed e–b_2 splittings. A plot of the calculated e–b_2 splitting vs. the experimental splitting is shown in Figure 12. The calculated splittings are larger than the observed value in each case, but the trend is reproduced well. The larger splittings are due in part to the fact that d functions were not included in the P basis set, so that the calculated π-acceptor abilities are less than expected. An additional calculation on $P(OMe)_3$ with P d orbitals showed only small changes in the eigenvalues and eigenvectors. We, therefore, feel justified in using this smaller basis set, even though the P d orbitals may play some part in the bonding.

Another particularly interesting aspect of these calculations is that they suggest that the alkylphosphines not only are poor π acceptors but may actually have some π-donor ability. One can see how this may arise by comparing the qualitative MO diagrams for the complexes of PF_3 and PMe_3 shown in Figure

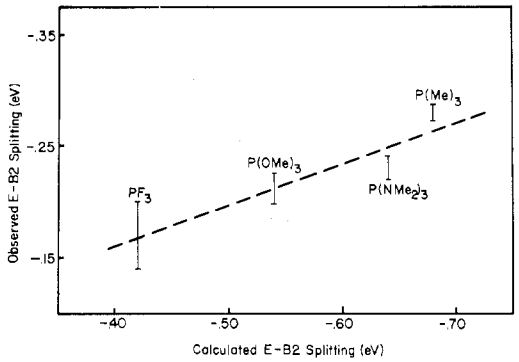

Figure 12. Observed vs. calculated e–b_2 splitting.

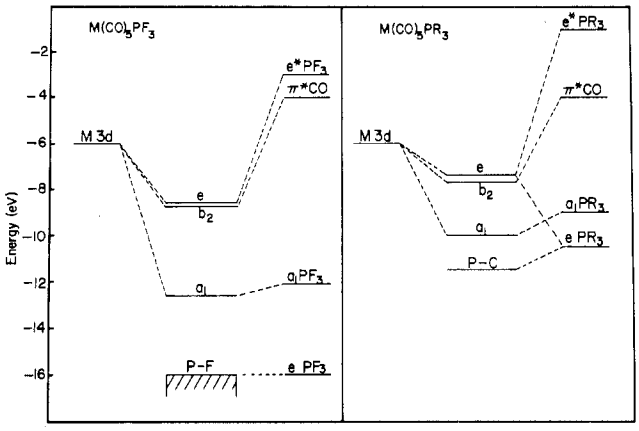

Figure 13. MO diagrams for $PF_3Cr(CO)_5$ and $PMe_3Cr(CO)_5$.

13. In both compounds the e*, which is the antibonding counterpart to the P–L set, is the π-acceptor orbital. This orbital is closer in energy to the metal e set in PF_3 than in PMe_3. Thus, PF_3 will accept more electron density from the metal. The bonding P–F e set is so low in energy in PF_3 that it will not interact with the metal e orbitals. However, the P–C e set is much closer to the metal levels in the PMe_3 compound. The calculations suggest that this e set, in fact, destabilizes the metal e levels and, in part, accounts for the large e–b_2 splitting observed in the alkylphosphines. Thus, the alkylphosphines are acting like π donors.

Conclusions

Photoelectron spectroscopy has been shown to be a valuable tool in studying phosphorus ligands and their transition-metal complexes. These studies established scales of relative π-acceptor ability, $PR_3 < P(NR_2)_3 < P(OR)_3 < PF_3$, and σ-donor strength, $PR_3 > P(OR)_3 > P(NR_2)_3 > PF_3$, with much higher precision than approximate CO force constant analysis. The order of π-acceptor abilities parallels the electronegativity of the P substituents, but the σ-donor strengths are influenced by the direct interaction of the substituents' lone pairs and P–L bond pairs. Our results show that PF_3 is a similar but somewhat poorer π acceptor than CO and that alkylphosphines may have some π-donor properties. The constancy of the tungsten spin–orbit coupling parameter illustrates the ability of the carbonyls to act as reservoirs for the π-electron density and to release these electrons as the π-acceptor strength of the other ligands changes. This latter result and the fairly large changes in the e–b_2 splitting in going from $M(CO)_6$ (0.00) to $PR_3M(CO)_6$ (−0.29) confirm the importance of π bonding in group 6B carbonyl systems.

Acknowledgment. The authors thank the Robert A. Welch Foundation (Grant A-648) for support of this work.

Registry No. $(PEt_3)Cr(CO)_5$, 21321-30-2; $(PEt_3)Mo(CO)_5$, 19217-79-9; $(PEt_3)W(CO)_5$, 21321-31-3; $(PMe_3)Cr(CO)_5$, 26555-

09-9; $(PMe_3)Mo(CO)_5$, 16917-96-7; $(PMe_3)W(CO)_5$, 26555-11-3; $(P(NMe_2)_3)Cr(CO)_5$, 15137-66-3; $(P(NMe_2)_3)Mo(CO)_5$, 14971-43-8; $(P(NMe_2)_3)W(CO)_5$, 19976-82-0; $(P(OEt)_3)Cr(CO)_5$, 18461-32-0; $(P(OEt)_3)Mo(CO)_5$, 15603-75-5; $(P(OEt)_3)W(CO)_5$, 23306-43-6; $(P(OMe)_3)Cr(CO)_5$, 18461-34-2; $(P(OMe)_3)Mo(CO)_5$, 15631-20-6; $(P(OMe)_3)W(CO)_5$, 23306-42-5; $(PF_3)Cr(CO)_5$, 18461-42-2; $(PF_3)Mo(CO)_5$, 15322-05-1; $(PF_3)W(CO)_5$, 18461-47-7.

References and Notes

(1) Robert A. Welch Foundation Postdoctoral Fellow.
(2) D. W. Turner, C. Baker, A. D. Baker, and C. R. Brundle, "Molecular Photoelectron Spectroscopy", Wiley-Interscience, London, 1970.
(3) M. B. Hall, *J. Am. Chem. Soc.*, **97**, 2057 (1975).
(4) (a) R. B. King, *Inorg. Chem.*, **2**, 936 (1963); (b) R. J. Clark and P. I. Hoberman, *ibid.*, **4**, 1771 (1965); (c) W. Strohmeier and F. J. Muller, *Chem. Ber.*, **100**, 2812 (1967); (d) D. J. Darensbourg and T. L. Brown, *Inorg. Chem.*, **7**, 959 (1968); (e) J. Dalton, I. Paul, J. G. Smith, and F. G. A. Stone, *J. Chem. Soc. A*, 1195, 1199 (1968); (f) H. Schumann, O. Stelzer, and U. Niederreuther, *J. Organomet. Chem.*, **16**, P64 (1969); (g) R. Mathieu, M. Lenzi, and R. Poilblanc, *Inorg. Chem.*, **9**, 2030 (1970); (h) H. Schumann, O. Stelzer, J. Kuhley, and U. Niederreuther, *Chem. Ber.*, **104**, 993 (1971); (i) R. B. King and T. F. Korenowski, *Inorg. Chem.*, **10**, 1188 (1971); (j) C. Barbeau and J. Turcotte, *Can. J. Chem.*, **54**, 1603 (1976).
(5) (a) F. Ogilvie, R. J. Clark, and J. G. Verkade, *Inorg. Chem.*, **8**, 1904 (1969); (b) R. L. Keiter and J. G. Verkade, *ibid.*, **8**, 2115 (1969); (c) M. S. A. Abd El-Mottaleb, *J. Mol. Struct.*, **32**, 203 (1976).
(6) B. R. Higginson, D. R. Lloyd, J. A. Connor, and I. H. Hillier, *J. Chem. Soc., Faraday Trans. 2*, 1418 (1974).
(7) (a) A. H. Cowley, D. W. Goodman, N. A. Kuebler, M. Sanchez, and J. G. Verkade, *Inorg. Chem.*, **16**, 854 (1977); (b) J. H. Hargis and S. D. Worley, *ibid.*, **16**, 1686 (1977).
(8) J. A. Connor, E. M. Jones, and G. K. McEwen, *J. Organomet. Chem.*, **43**, 757 (1972).
(9) H. Meerwein, *Org. Synth.*, **46**, 113 (1966).
(10) E. W. Abel, I. S. Butler, and J. G. Reid, *J. Chem. Soc.*, 2068 (1963).
(11) M. B. Hall and R. F. Fenske, *Inorg. Chem.*, **11**, 768 (1972).
(12) J. W. Richardson, W. C. Nieuwpoort, R. R. Powell, and W. F. Edgell, *J. Chem. Phys.*, **36**, 1057 (1962).
(13) R. F. Fenske and D. D. Radtke, *Inorg. Chem.*, **7**, 479 (1968).
(14) E. Clementi, *J. Chem. Phys.*, **40**, 1944 (1964); *IBM J. Res. Dev.*, **9**, 2 (1965).
(15) Y. Morino, K. Kuchitsu, and T. Moritani, *Inorg. Chem.*, **8**, 867 (1969); G. C. Holywell, D. W. H. Rankin, B. Beagley, and J. M. Freeman, *J. Chem. Soc. A*, 785 (1971); L. J. Vandegriend, J. C. Clardy, and J. G. Verkade, *Inorg. Chem.*, **14**, 710 (1975).
(16) R. C. Weast, Ed., "Handbook of Chemistry and Physics", Chemical Rubber Publishing Co., Cleveland, Ohio, 1966.
(17) H. J. Plastas, J. M. Stewart, and S. O. Grimm, *J. Am. Chem. Soc.*, **91**, 4326 (1969).
(18) J. F. Nixon, *J. Chem. Soc., Dalton Trans.*, 2226 (1973); R. A. Head, J. F. Nixon, G. J. Sharp, and R. J. Clark, *ibid.*, 2054 (1975).
(19) W. A. G. Graham, *Inorg. Chem.*, **7**, 315 (1968).
(20) F. A. Cotton and C. S. Kraihanzel, *J. Am. Chem. Soc.*, **84**, 4432 (1962).
(21) J. A. Connor, *J. Organomet. Chem.*, **94**, 195 (1975).

Contribution from the Chemistry Division, Argonne National Laboratory, Argonne, Illinois 60439

Matrix-Isolation Spectroscopy of Aluminum, Copper, and Nickel Hydrides and Deuterides Produced in a Hollow-Cathode Discharge

R. B. WRIGHT,* J. K. BATES, and D. M. GRUEN

Received November 15, 1977

By use of the technique of matrix-isolation spectroscopy in conjunction with a hollow-cathode sputtering source the infrared-active vibrations of the diatomic hydrides and deuterides of aluminum, copper, and nickel have been directly observed. The metal hydride and deuteride vibrations at 14 K in an argon matrix occurred as follows: AlH, 1593 cm^{-1}; AlD, 1158 cm^{-1}; CuH, 1882 cm^{-1}; CuD, 1356 cm^{-1}; NiH, 1906 cm^{-1}; NiD, 1374 cm^{-1}.

I. Introduction

Recent interest in the possible production and detection of metal hydrides and deuterides arising from physical/chemical sputtering of metals by energetic reactive ion beams is related to the plasma first-wall interactions envisioned to occur in thermonuclear reactors. Sputtering of the first wall by ions and/or neutrals escaping from the plasma can lead to serious first-wall erosion as well as plasma contamination problems. Therefore, the qualitative and quantitative detection of the sputtered products resulting from bombardment of a metal surface by energetic hydrogen and deuterium ions is essential to ascertain the extent of these problems and the possible solutions thereof.

A convenient method for producing diatomic metal hydride and deuteride molecules would also be useful for a detailed examination of the elementary steps involved in catalytic reactions. Recent work on matrix-isolated ethylene[1a] as well as nickel- and platinum–ethylene complexes[1b] has shown the close relationship between the spectroscopic properties of matrix-isolated complexes and the spectroscopy of chemisorbed species on metal surfaces. To investigate intermediates in catalytic hydrogenation reactions, the program would be to matrix-isolate metal hydrides together with ethylene for example and to search for reaction products on the way to ethane. The hollow-cathode discharge method for the production of metal hydrides has some advantages over the more conventional method using thermally generated H or D beams. As will become apparent, the discharge method also appears to have some disadvantages, particularly with regard to the large M/MH ratios observed in the matrices.

The technique and utility of matrix-isolation spectroscopy has been well documented in the literature[2-5] demonstrating that it is a viable technique for the optical study of atomic and molecular (stable or unstable) species. Hollow-cathode sputtering sources where the metal atoms are sputtered from the surface of the cathode by a low-energy plasma and subsequently excited in the discharge to produce an atomic spectrum have been used for many years.[6] If small amounts of a reactive gas are added to the discharge, molecular species formed by reactions with the sputtered metal atoms can occur.[7-9] In this paper, the technique of matrix-isolation spectroscopy has been utilized to detect by infrared absorption the formation of aluminum, copper, and nickel diatomic hydrides and deuterides produced in a hollow-cathode cathode discharge. This technique permits, at present, the qualitative determination of the sputtered products resulting from a low-energy reactive plasma interaction with a metal surface using UV–visible and infrared absorption detection of the matrix-isolated sputtered species.

II. Experimental Section

A cross-sectional view of the hollow-cathode sputtering source and matrix-isolation collection assemblies is shown in Figure 1. The hollow-cathode sputtering source is similar to one which has been previously used in our laboratory;[9] the present source has been modified for easier use and reliability. A Cryogenic Technology, Inc., Model 21 closed-cycle helium refrigerator (b) enclosed by a stainless steel

0020-1669/78/1317-2275$01.00/0